IOP Conf. Series: Materials Science and Engineering **305** (2018) 012007 doi:10.1088/1757-899X/305/1/012007

Modeling of Lithium Niobate ($LiNbO_3$) and Aluminum Nitride (AlN) Nanowires Using Comsol Multiphysics Software: The Case of Pressure Sensor

A.A. Ahmad[*1], A. Alsaad[1], Q.M. Al-Bataineh[1], M.A. Al-Naafa[2]

[1]*Department of Physical Sciences, Jordan University of Science and Technology, P. O. Box 3030, Irbid 22110, Jordan.*
[2]*Department of Chemical Engineering, University of Hafr Albatin Saudi Arabia*

sema@just.edu.jo

Abstract In this study, Lithium niobate ($LiNbO_3$) and Aluminum nitride (AlN) nanostructures were designed and investigated using the COMSOL Multiphysics software for pressure sensing applications. The Finite Element Method (FEM) was used for solving the differential equations with various parameters such as size, length, force, etc. The variation of the total maximum displacement as a function of applied force for various NWs lengths and the variation of the voltage as a function of applied force were plotted and discussed. AlN nanowires exhibit a better piezoelectric response than $LiNbO_3$ nanowires do.

Keywords: Piezoelectricity, Nanoelectromechanical system, COMSOL Multiphysics, Finite Element Method, Piezoelectric response

1. Introduction

Piezoelectricity is a direct electrical-mechanical conversion in certain types of crystals. It has many applications since the discovery by the Curie brothers in 1880 [1]. The reverse piezoelectric effect is observed in several crystals when an applied voltage causes bending in the crystal. The Micro Electro-Mechanical Systems MEMS were some of the most interesting applications in recent years. Crystal deformation does not exceed few nanometers, but the force exerted on the crystal to induce the deformation is in the order of few mega-newtons. For example, one cubic centimeter cube of quartz generates 12 kV with a two kilo-newtons applied force but at low current [2]. Piezoelectric devices contain materials where electric charge is created due to mechanical stress. Piezoelectric devices module based on Finite Element Method (FEM) implemented in commercial software COMSOL Multiphysics is used to study devices such as Micro Electro-Mechanical Systems (MEMS), bio sensors, controllers or Micro Machined Modal Gyroscopes [3-4]. Applications such as energy harvesting have been presented in several previous works [5-8]. Energy harvesting is an evolving area of research where unexploited energy is converted into beneficial electrical power consequently offering a promising solution to the environmental and substitution issues associated with battery powered systems. The recent advancement of micro fabrication technology has led to increasing interest in developing micro-energy harvesters in the form of MEMS devices.

In the current study, we focus on Lithium niobate ($LiNbO_3$) and Aluminum nitride (AlN) which are key candidate materials in integrated optical circuits due to their photo-stability, as well as, excellent nonlinear optical properties including large piezoelectric, electro-optic, and nonlinear optical coefficients [9-11]. The single crystal of $LiNbO_3$ lacks inversion symmetry and thus exhibits ferroelectricity, Pockels effect, piezoelectric effect, photo-elasticity and nonlinear optical polarizability [12]. $LiNbO_3$ has attracted much attention due to its potential in applications such as optical waveguides, cell phones, piezoelectric sensors, optical modulators and various other linear and non-linear optical applications [13]. In addition, we investigated the compound under ambient temperature and pressure. The AlN compound crystallizes in the hexagonal wurtzite structure (w-AlN) which belongs to the *P63mc* space group. The w-AlN is a relatively wide-band-gap semiconductor that has attracted increasing interest because of its low compressibility, good thermal stability, chemical and radiation inertness, and applications such as short-wavelength light emitting diodes, optical detectors, high-pressure, high temperature, and high-frequency optoelectronic devices [14-16]. Furthermore, because of the excellent piezoelectric response of w-AlN, it is used for surface acoustic wave sensors (SAWs) deposited on silicon wafers. One application of SAWs is an RF filter which is widely used in cell phones. The w-AlN is also used to build piezoelectric micro machined ultrasound transducers, which emit and receive ultrasound and can be used for in-air range finding over distances of up to a meter [17-19]. In this study, we use COMSOL Multiphysics software (version 5.1) that can be used to account for coupled or Multiphysics phenomena [20] to investigate the piezoelectric properties of $LiNbO_3$ and AlN systems. In particular, we determine the piezoelectric potential distributions in different geometries of $LiNbO_3$ and AlN systems at the nanoscale range. Specifically, we consider the case of nanowires (NWs) designed pressure sensors.

2. Theoretical Consideration

In general case, Hooke's law can be expressed as:

$\varepsilon_{ij} = S_{ijkl}\tau_{kl}$ …….. (1)

where ε_{ij} and τ_{kl} denote the strain and stress tensors, respectively.$S_{ijkl}$is the compliance, and it is fourth-rank tensor quantity. The direct consequence of the symmetry in the strain and the stress tensors is that only 36 components of the compliance tensor are independent and distinct terms, instead of 81 components of the compliance tensor. The relation between the stress and the strain can be simplified through applying the Voigt notation as the following [21]:

$\varepsilon_i = S_{ij}\tau_j$ ……..... (2)

Because of the symmetry in the compliance tensor for the general anisotropic linear elastic solid, there are 21 independent elastic constants. By considering the symmetry conditions found in the wurtzite crystal structure of the AlN NWs, the stress-strain relations are expressed as (the z-axis is the c-axis for wurtzite crystal):

$$\begin{pmatrix}\varepsilon_1\\ \varepsilon_2\\ \varepsilon_3\\ \varepsilon_4\\ \varepsilon_5\\ \varepsilon_6\end{pmatrix} = \begin{pmatrix} S_{11} & S_{12} & S_{13} & 0 & 0 & 0\\ S_{12} & S_{11} & S_{13} & 0 & 0 & 0\\ S_{13} & S_{13} & S_{33} & 0 & 0 & 0\\ 0 & 0 & 0 & S_{44} & 0 & 0\\ 0 & 0 & 0 & 0 & S_{44} & 0\\ 0 & 0 & 0 & 0 & 0 & 2(S_{11}-S_{12}) \end{pmatrix}\begin{pmatrix}\tau_1\\ \tau_2\\ \tau_3\\ \tau_4\\ \tau_5\\ \tau_6\end{pmatrix}$$ .. (3) is 2 in the last row superscript or factor? 2(S1-S)?

The elastic modulus (Young's modulus) in remarkable crystallographic directions can be extracted from the compliance matrix using the following equations:

$E_{[2\bar{1}\bar{1}0]} = \tau_1/\varepsilon_1 = (S_{11})^{-1}$ …….. (4)

$E_{[01\bar{1}0]} = \tau_2/\varepsilon_2 = (S_{11})^{-1}$ …….. (5)

$E_{[0001]} = \tau_3/\varepsilon_3 = (S_{33})^{-1}$ ……...(6)

The crystals that lack inversion symmetry exhibits piezoelectric effect and produce an electric polarization in response to mechanical stress as follow:

$P_n = e_{nj}\varepsilon_j$ ……...(7)

Where P_n(n = 1, 2, 3) are the components of the polarization vector that is created as a result of piezoelectric effect, ε_j(j = 1, 2, 3, 4, 5, 6) are the components of the strain tensor, e_{nj} is the tensor of the stress constants using Voigt notation. For the wurtzite structure of AlN, the matrix of the piezoelectric stress constants can be written as [22]:

$$e_{nj} = \begin{pmatrix} 0 & 0 & 0 & 0 & e_{15} & 0\\ 0 & 0 & 0 & e_{15} & 0 & 0\\ e_{31} & e_{31} & e_{33} & 0 & 0 & 0 \end{pmatrix}$$ ……. (8)

The matrix has only three independent elements. The converse piezoelectric effect describes how an applied electric field (E_k) will create a resultant strain (ε_i) which leads to a physical deformation of the material. The converse piezoelectric effect in Voigt notation can be written as:

$$\varepsilon_i = d_{ki} E_k \qquad \text{..... (9)}$$

Where d_{ki} is the tensor of the piezoelectric strain constants. For the hexagonal wurtzite crystal it is given by:

$$d_{ki} = \begin{bmatrix} 0 & 0 & d_{31} \\ 0 & 0 & d_{31} \\ 0 & 0 & d_{33} \\ 0 & d_{15} & 0 \\ d_{15} & 0 & 0 \\ 0 & 0 & 0 \end{bmatrix} \qquad \text{..... (10)}$$

The relationship between strain tensor, stress tensor, electric displacement(D_n) and electric field for a linear piezoelectric material can be given by the constitutive equations [23].

$$\varepsilon_i = S_{ij}^E \tau_j + d_{ni} E_n \qquad \text{..... (11)}$$

$$D_n = d_{ni}\tau_i + \xi_{ik}^{\tau} E_k \qquad \text{..... .(12)}$$

Where the indexes i, j = 1, 2, .. 6 and n, k = 1, 2, 3 refer to different directions within the material coordinate system, and ξ_{ik} is the permittivity tensor.

Piezoelectric materials can generate electrical voltage when uniaxial strain is applied. For low frequency applications at constant temperature, the direct piezoelectric effect can be described by:

$$\vec{D} = d_1 \vec{T} + \varepsilon^T \vec{E} \qquad \text{..... (13)}$$

$$\vec{S} = s^E \vec{T} + d_2 \vec{E} \qquad \text{.....(14)}$$

$\vec{D}$: Electric displacement and d_1 and d_2 are piezoelectric charge coefficients for the direct piezoelectric effect and the converse piezoelectric effect, respectively.

$\vec{T}$ denotes the mechanical stress.

ε^T: Permittivity at constant stress.

$\vec{E}$: Electric field.

$\vec{S}$: Mechanical strain

S^E: Mechanical compliance

Equation (13) describes the electrical field conversion into mechanical stress and equation (14) depicts the mechanical stress conversion into electrical field.

3. COMSOL Multiphysics Simulation

To simulate the pressure sensors using COMSOL Multiphysics, the piezoelectric devices Multiphysics interface has to be chosen. Solid mechanics and electrostatics are combined within the piezoelectric devices Multiphysics interface with the constitutive relationships required to model the piezoelectric device.

3.1 Geometric Modeling

3D geometry is considered for the simulations. The piezoelectric device contains a thin film deposited on silicon wafers with dimensions of 200 x 200 x 10 nm and nine NWs seeded on it. Each of the NWs has a radius of 10 nm. The height of the NWs has been varied in steps of 100, 150 and 200 nm, as shown in figure 1. The geometry has been chosen because experimental combination of electrodeposition and polymeric templates followed by chemical etching provides a large variety nanowires of controlled size, geometry, composition, and surface morphology very close to our chosen geometry..

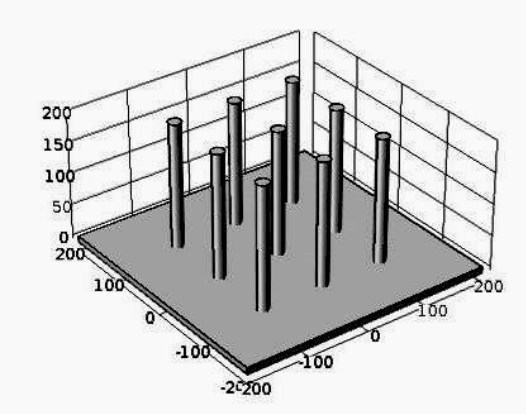

Figure 1: The geometry of piezoelectric device.

3.2 Meshing

Before starting simulation, the NW was broken into small areas; each is called a “mesh”. The mesh is composed of (14809, 17725 and 21044) tetrahedral elements and (7952, 9464 and 10806) triangular elements for (100, 150 and 200) nm height of NWs, respectively. The mesh is created using the mapped mesh tool with a physics-controlled mesh and normal mesh element size. For instance, figure 2 illustrates the obtained mesh for a NW of height 200 nm.

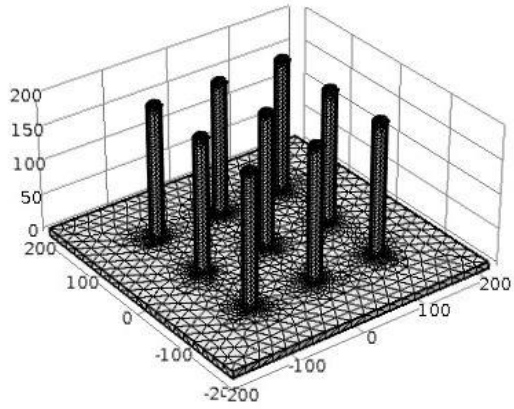

Figure 2: Piezoelectric device mesh for a NW of height 200 nm.

3.3 Sub-domain Settings

The structure of the simulated piezoelectric device consists of two compounds; the first is $LiNbO_3$ and has the following matrices and parameters:
Compliance matrix

$$S^E = \begin{pmatrix} 5.78 & -1.01 & -1.47 & -1.02 & 0 & 0 \\ -1.01 & 5.78 & -1.47 & 1.02 & 0 & 0 \\ -1.47 & -1.47 & 5.02 & 0 & 0 & 0 \\ -1.02 & 1.02 & 0 & 17 & 0 & 0 \\ 0 & 0 & 0 & 0 & 17 & -2.04 \\ 0 & 0 & 0 & 0 & -2.04 & 13.6 \end{pmatrix} * 10^{-12}\, m^2 / N$$

piezoelectric Coupling

$$d = \begin{pmatrix} 0 & 0 & 0 & 0 & 68 & -42 \\ -21 & 21 & 0 & 68 & 0 & 0 \\ -1 & -1 & 6 & 0 & 0 & 0 \end{pmatrix} * 10^{-12}\ C / N$$, relative permittivity matrix

and density $\rho = 4700\, Kg / m^3$. The corresponding matrices and parameters for the AlN compound are given as:

Compliance matrix

$$S^E = \begin{pmatrix} 28.58 & 08.99 & -3.83 & 0 & 0 & 0 \\ -8.99 & 31.17 & -9.65 & 0 & 0 & 0 \\ -3.83 & -9.65 & 30.38 & 0 & 0 & 0 \\ 0 & 0 & 0 & 80 & 0 & 0 \\ 0 & 0 & 0 & 0 & 80 & 0 \\ 0 & 0 & 0 & 0 & 0 & 80 \end{pmatrix} *10^{-13} \quad m^2/N$$

, piezoelectric Coupling

$$d = \begin{pmatrix} 0 & 0 & -1.73 & 0 & 0 & -2.78 \\ 0 & 0 & 5.49 & 0 & -3.84 & 0 \\ -3.84 & 0 & 0 & 0 & 0 & 0 \end{pmatrix} *10^{-12} \; C/N$$

, relative permittivity matrix

$$\varepsilon_r = \begin{pmatrix} 9.2 & 0 & 0 \\ 0 & 9.2 & 0 \\ 0 & 0 & 10.3 \end{pmatrix}$$

and density, $\rho = 3300 \; Kg/m^3$.

3.4 Boundary Settings

The base of our simulated piezoelectric device is made of a fixed substrate, on the top of which a NW is seeded. The upper end of the NW is taking to be free in response to the applied force. The base of our piezoelectric device is considered to be electrically grounded. The remaining parts of our piezoelectric device are kept at zero charge/symmetry conditions.

3.5 Simulation Results: three different kinds of forces: $F = F_0\hat{x}$ as a lateral force, $F = F_0\hat{z}$ have been applied as a tensile force and $F = -F_0\hat{z}$ as a compressive force, as displayed in Figure 3.

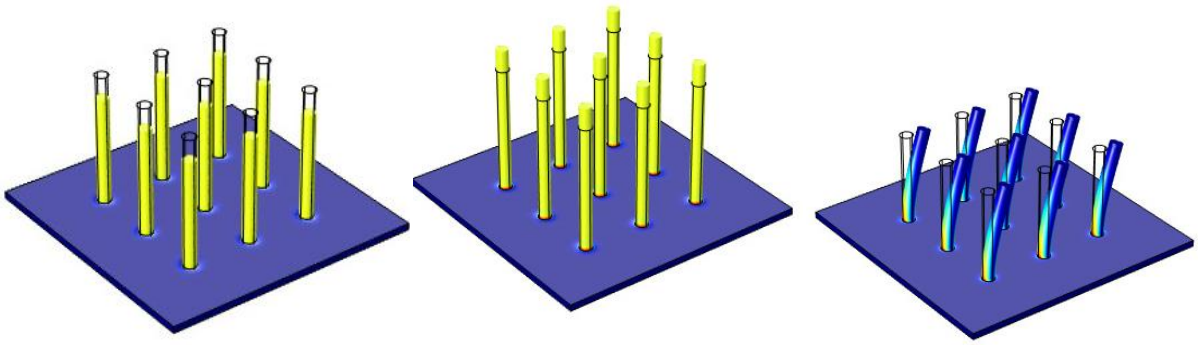

Figure 3: The three different applied forces in our study are: (a) Lateral force, $F = F_0\hat{x}$ (b) Tensile force, $F = F_0\hat{z}$ and (c) Compressive force, $F = F_0\hat{z}$.

4. Results and Discussions

In this section, we describe and interpret our results on the piezoelectric output potential and deformation (displacement) behavior of the ($LiNbO_3$) and (AlN) NWs as functions of different applied forces. We study three different heights of $LiNbO_3$ and AlN nanowires, namely 100 nm, 150 nm and 200 nm.

4.1 Nanowires of height (100) nm

Figure 4 shows the effect of the force F_x applied at the top free end perpendicular to the left side of $LiNbO_3$ and AlN NWs for a NW height of 100 nm. A maximum total displacement of 2.0983 nm for $LiNbO_3$ and 1.2705 nm for AlN at (F_x = 90 nN) was observed at the bottom of the NW from the left side. However, maximum piezoelectric potentials of 44.5 mV and 50.3 mV were observed at the left edge surface of the NWs for $LiNbO_3$ and AlN NWs, respectively.

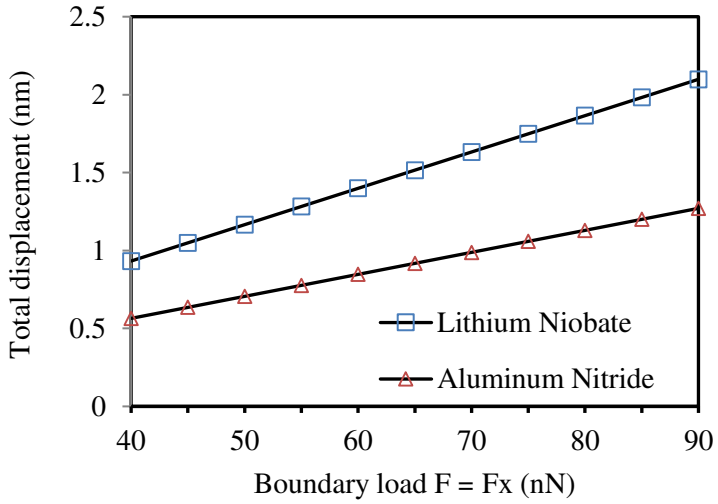

Figure 4: Total displacement (nm) of $LiNbO_3$ and AlN with boundary load F = F_x (nN) for 100 nm height NWs.

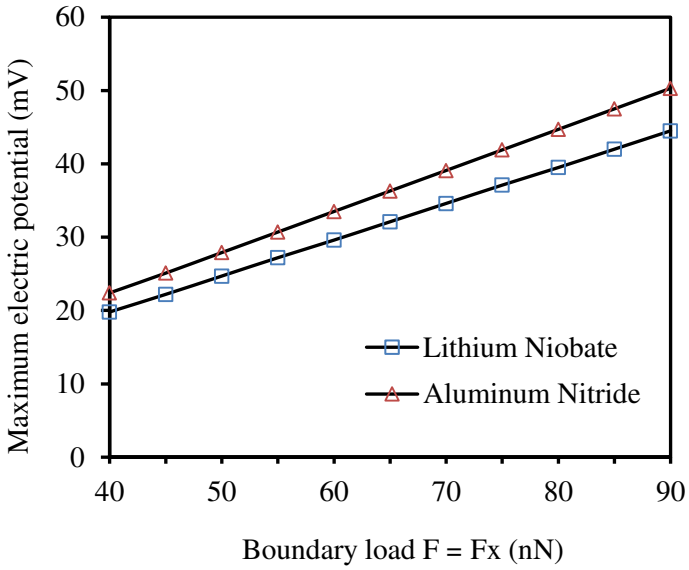

Figure 5: Maximum electric potential (mV) of $LiNbO_3$ and AlN with boundary load F = F_x (nN) for 100 nm height NWs.

In addition, figures 4 and 5 clearly indicate that for the range of 40 nN to 90 nN applied force, both total displacement and electric potential exhibit a linear relationship as functions of applied load. In addition, figures 4 and 5 indicate that, for the same boundary load, $LiNbO_3$ NWs undergo total displacement larger than the one exhibited by AlN NWs. On the other hand, AlN NWs undergo maximum electric potential larger the one exhibited by $LiNbO_3$ NWs. This remarkable result indicates that AlN piezoelectric response is better than that of $LiNbO_3$ system. Furthermore, we found that, when the force F_z is applied compressively or tensely over the upper surface of $LiNbO_3$ and AlN NWs, the total displacement as a function of the boundary load remains linear as clearly displayed in figure 6.

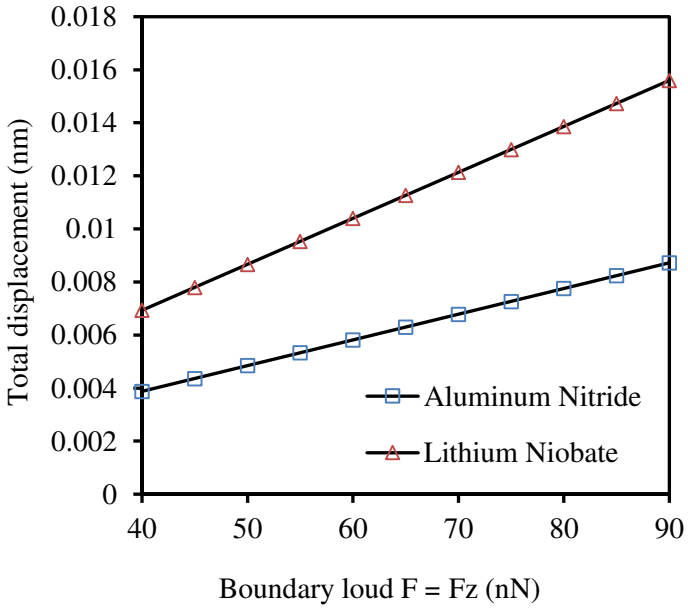

Figure 6: Total displacement (nm) of $LiNbO_3$ and AlN with boundary load F=F_z (nN) for 100 nm height NWs.

Moreover, we studied the dependence of piezoelectric potential on the applied force F_z in the range of 40 nN to 90 nN for both NWs. Figure 7 shows piezoelectric potential as a function of applied force. The generated piezoelectric potentials exhibit positive values for tension forces and negative values for compressive forces for both NWs.
For instance, figure 7 shows that when F_z = 90 nN was applied, maximum piezoelectric potentials of ±73 mV and ±187 mV were generated at the top surface of $LiNbO_3$ and AlN NWs, respectively.

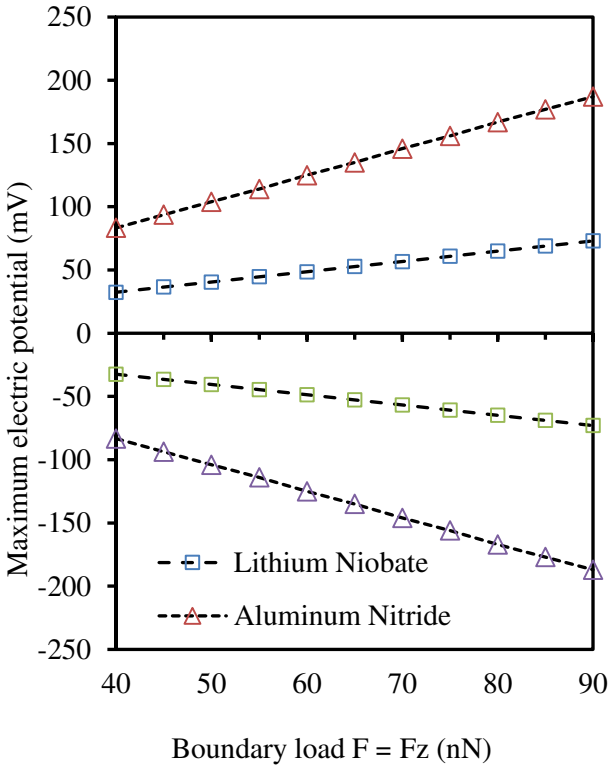

Figure 7: Maximum electric potential (mV) of $LiNbO_3$ and AlN with boundary load F = F_z (nN) for 100 nm height NWs (Positive sign for tension force and negative for compressive force).

4.2 Nanowires of height (150) nm

Figure 8 shows the effect of the force F_x applied at the top free end perpendicular to the left side of $LiNbO_3$ and AlN NWs for a NW height of 150 nm. A maximum total displacement of 7.0705 nm for $LiNbO_3$ and 4.2807 nm for AlN at (F_x = 90 nN) was observed at the bottom of the NW from the left side. However, maximum piezoelectric potentials of 72.5 mV and 84.7 mV were observed for $LiNbO_3$ and AlN NWs, respectively, at the left edge surface of the NWs.

In addition, Figures 8 and 9 clearly indicate that for the range of 40 nN to 90 nN applied force, both total displacement and electric potential exhibit a linear relationship.

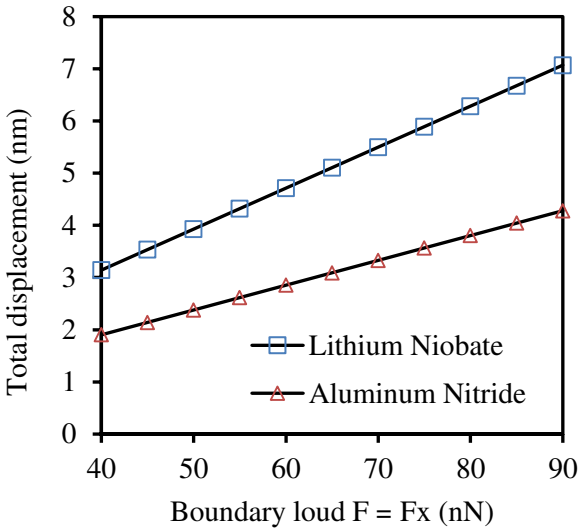

Figure 8: Total displacement (nm) of $LiNbO_3$ and AlN with boundary load F = F_x (nN) for 150 nm height NWs.

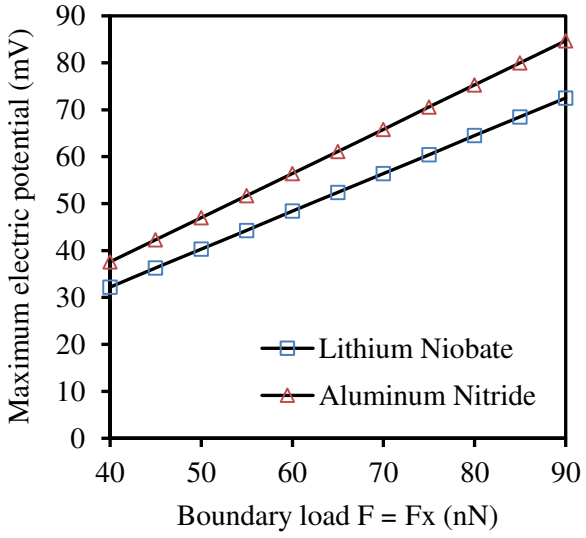

Figure 9: Maximum electric potential (mV) of $LiNbO_3$ and AlN with boundary load F=F_x (nN) for 150 nm height NWs.

We have found that when the force F_z is applied compressively or tensely over the upper surface of $LiNbO_3$ and AlN NWs, the total displacement as a function of the boundary load remains linear as clearly displayed in figure 10.

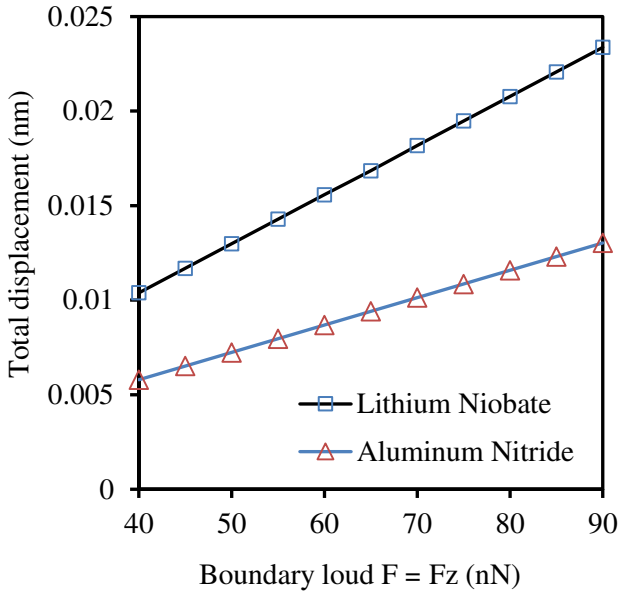

Figure 10: Total displacement (nm) of $LiNbO_3$ and AlN with boundary load $F=F_z$ (nN) for 150 nm height NWs.

Moreover, we studied the dependence of piezoelectric potential on the applied force F_z in the range 40 nN to 90 nN for both NWs. Figure 10 shows piezoelectric potential as a function of applied force. In addition, figure 11 shows that the generated piezoelectric potentials exhibit positive values for tension forces and negative values for compressive forces for both NWs. For instance, when $F_z = 90$ nN was applied, maximum piezoelectric potentials of ±109 mV and ±283 mV were generated at the top surface of $LiNbO_3$ and AlN NWs, respectively. Furthermore, figure 11 indicates that the generated piezoelectric potential exhibits a positive slope linear relationship with the applied tension boundary load and an equal but negative slope linear relationship with the applied compressive load.

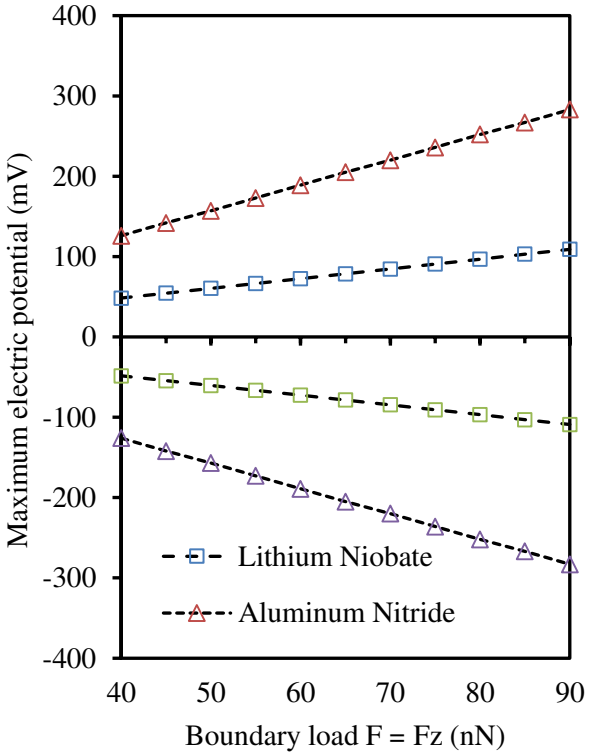

Figure 11: Maximum electric potential (mV) of $LiNbO_3$ and AlN with boundary load $F=F_z$ (nN) for 150 nm height NWs (Positive sign for tension force and negative for compressive force).

4.3 Nanowires of height (200) nm

Figure 12 shows the effect of the force F_x applied at the top free end perpendicular to the left side of $LiNbO_3$ and AlN NWs for a NW height of 200 nm. A maximum total displacement of 16.791 nm for $LiNbO_3$ and 10.164 nm for AlN at (F_x = 90 nN) was observed at the bottom of the NW from the left side. However, maximum piezoelectric potentials of 100 mV and 118 mV were observed for $LiNbO_3$ and AlN NWs, respectively, at the left edge surface of the NWs.

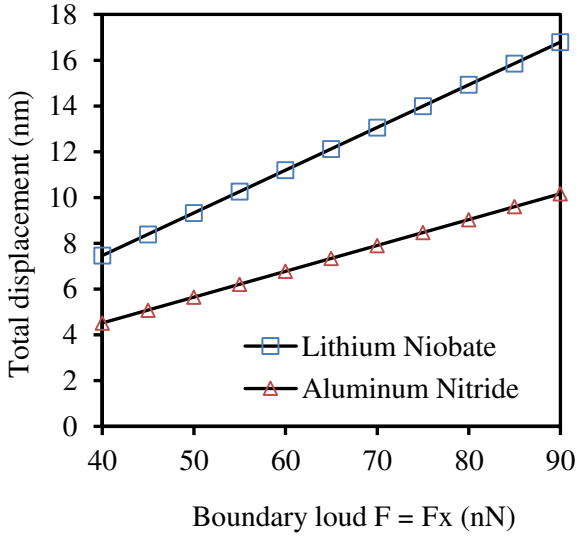

Figure 12: Total displacement (nm) of $LiNbO_3$ and AlN with boundary load $F=F_x$ (nN) for 200 nm height NWs.

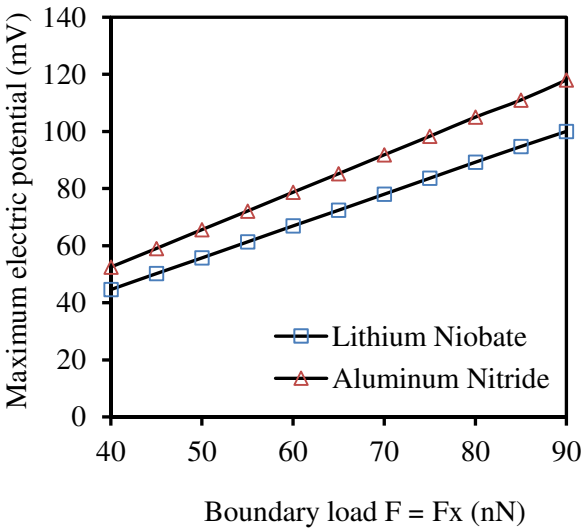

Figure 13: Maximum electric potential (mV) of $LiNbO_3$ and AlN with boundary load $F=F_x$ (nN) for 200 nm height NWs.

In addition, Figures 12 and 13 clearly indicate that for the range of 40 nN to 90 nN applied force, both total displacement and electric potential exhibit a linear relationship.

We have found that when the force F_z is applied compressively or tensely over the upper surface of $LiNbO_3$ and AlN NWs, the total displacement as a function of the boundary load remains linear as clearly shown in figure 14.

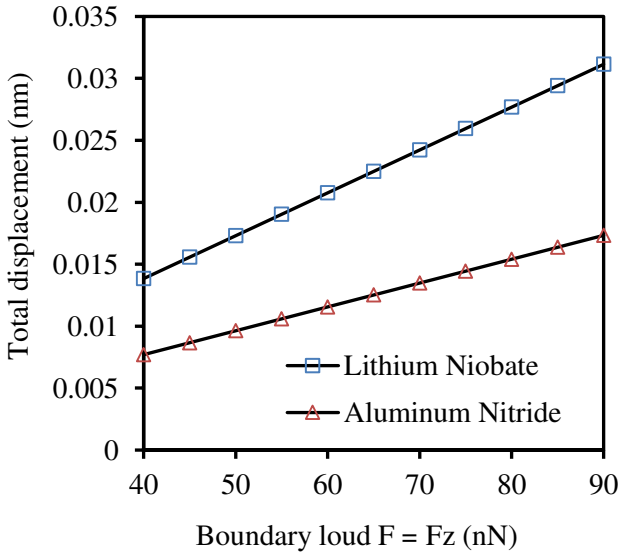

Figure 14: Total displacement (nm) of $LiNbO_3$ and AlN with boundary load $F=F_z$ (nN) for 200 nm height NWs.

Moreover, we studied the dependence of piezoelectric potential on the applied force F_z in the range 40 nN to 90 nN for both NWs. Figure 15 shows piezoelectric potential as a function of applied force.

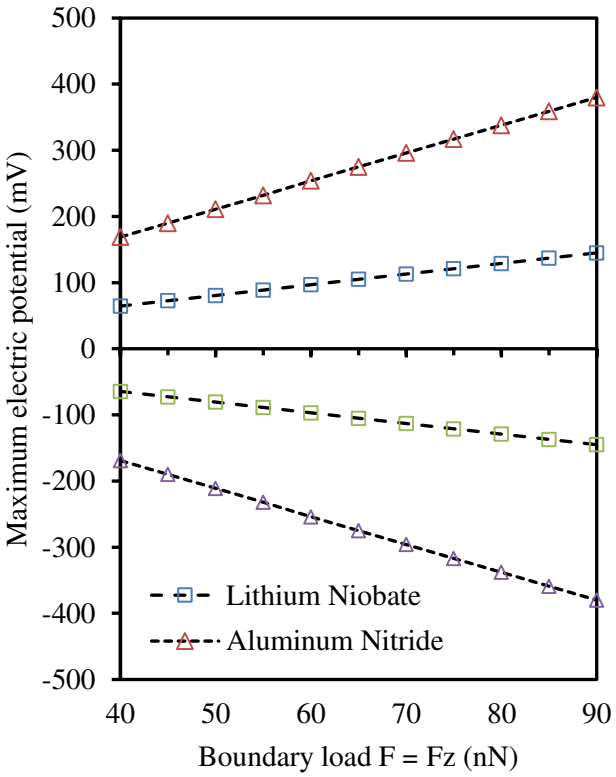

Figure 15: Maximum electric potential (mV) of $LiNbO_3$ and AlN with boundary load $F=F_z$ (nN) for 200 nm height NWs (Positive sign for tension force and negative for compressive force).

The generated piezoelectric potentials exhibit positive values for tension forces and negative values for compressive forces for both NWs. For instance, when F_z = 90 nN was applied, maximum piezoelectric potentials of ±145 mV and ±380 mV were generated at the top surface of $LiNbO_3$ and AlN NWs, respectively.

5. Conclusion

In summary, Lithium niobate ($LiNbO_3$) and Aluminum nitride (AlN) nanowires with rod geometry were investigated using COMSOL Multiphysics based on the Finite Element Method (FEM). We found that $LiNbO_3$ nanowires undergo total displacement higher than the corresponding displacement exhibited by AlN wires under the same boundary loads. However, AlN nanowires piezoelectric response is higher than the corresponding response of $LiNbO_3$ nanowires as indicated by the higher piezoelectric potentials exhibited by AlN nanowires as compared with those of $LiNbO_3$ nanowires. This remarkable finding indicates that AlN nanowires exhibit a better piezoelectric response than $LiNbO_3$ under the same boundary loads. Furthermore, we found that in both nanowires, the tension and compressive loads generate higher total displacements and piezoelectric potentials than the corresponding total displacements and potentials produced by lateral loads. One of the main findings of this work is that, total displacement and generated piezoelectric potential in both nanowires depend mainly on the height of the nanowires used in the rod geometry. We found that the 200 nm height nanowire exhibit optimized total displacement and piezoelectric response when subjected to tension, compressive or lateral boundary loads for AlN and $LiNbO_3$ nanowires. Based on our findings, we find that the piezoelectric response of both nanowires is very

sensitive to the height of the nanowire in rod geometry particularly for AlN nanowires. Therefore, we recommend using the 200 nm height AlN nanowire in rod geometry for fabrication of piezoelectric and pressuring sensor devices.

Acknowledgments
The first three authors would like to acknowledge the technical and financial support provided by the faculty of scientific research at Jordan University of Science and Technology (JUST). The fourth author would like to acknowledge the support of the University of Hafr Albatin in Saudi Arabia.

References

[1] Karabalin RB, Matheny MH, Feng XL, Defay E, Le Rhun G, Marcoux C, Hentz S, Andreucci P, Roukes ML, *Piezoelectric nanoelectromechanical resonators based on aluminum nitride thin films.* Applied Physics Letters, 2009 **95(10)** 103111.
[2] Design M, *Sensor Sense: Piezoelectric Force Sensors.* Penton Media, 2008.
[3] Ayazi F, *The HARPSS process for fabrication of precision MEMS inertial sensors.* Mechatronics, 2002 **12(9)** 1185-1199.
[4] Wu X, Chen W, Zhang W, Lu Y, Cui F, Zhao X, editors. *Modeling analysis of piezoelectric micromachined modal gyroscope (PMMG)*. in *Nano/Micro Engineered and Molecular Systems, 2009. NEMS 2009 4th IEEE International Conference on*. 2009. IEEE.
[5] Beeby SP, Tudor MJ, and White N, *Energy harvesting vibration sources for microsystems applications.* Measurement science and technology, 2006 **17(12)** R175.
[6] Reddy VM and Kumar GVS, Multiphysics, *Design and analysis of microcantilevers with various shapes using comsol multiphysics software.* 2013 3(3) 681-684 .
[7] Jeon YB, Sood R, Jeong JH, Kim SG., *MEMS power generator with transverse mode thin film PZT.* Sensors and Actuators A: Physical, 2005 **122(1)** 16-22.
[8] Chhabra P, Sharma A, editors. *Design, Simulation and Fabrication of Piezoelectric Energy Harvester for an Application in Tire Pressure Monitoring System (TPMS)*. in *1st Winter Workshop on "Engineering at Nanoscale: From Materials to Bio-Sensors" IIT Indore*. 10. Dec. 2012.
[9] Yun BK, Park YK, Lee M, Lee N, Jo W, Lee S, et al., *Lead-free LiNbO3 nanowire-based nanocomposite for piezoelectric power generation.* Nanoscale research letters, 2014 **9(1)** 1-7.
[10] Santulli AC, Zhou H, Berweger S, Raschke MB, Sutter E, Wong SS, *Synthesis of single-crystalline one-dimensional LiNbO 3 nanowires.* CrystEngComm, 2010 **12(10)** 2675-2678.
[11] He JH, Yang RS, Chueh YL, Chou LJ, Chen LJ, Wang ZL, *Aligned AlN Nanorods with Multi-tipped Surfaces—Growth, Field-Emission, and Cathodoluminescence Properties.* Advanced Materials, 2006 **18(5)** 650-654.
[12] Volk T. and Wöhlecke M, *Lithium niobate: defects, photorefraction and ferroelectric switching*. Vol. 115. 2008: Springer Science & Business Media.
[13] Grigas A. and Kaskel S, *Synthesis of LiNbO3 nanoparticles in a mesoporous matrix.* Beilstein journal of nanotechnology, 2011 **2(1)** 28-33.
[14] Strite S. and Morkoç H, *GaN, AlN, and InN: a review.* Journal of Vacuum Science & Technology B, 1992 **10(4)** 1237-1266.

[15] Stampfl C. and Van de Walle C, *Density-functional calculations for III-V nitrides using the local-density approximation and the generalized gradient approximation.* Physical Review B, 1999 **59(8)** 5521.
[16] Berger, L.I., *Semiconductor materials*. 1996: CRC press.
[17] Przybyla RJ, Tang H-Y, Shelton SE, Horsley DA, Boser BE, editors. *12.1 3D ultrasonic gesture recognition*. in *Solid-State Circuits Conference Digest of Technical Papers (ISSCC), 2014 IEEE International*. 2014. IEEE.
[18] Ahmadi A, Hadipour NL, Kamfiroozi M, Bagheri Z, T*heoretical study of aluminum nitride nanotubes for chemical sensing of formaldehyde.* Sensors and Actuators B: Chemical, 2012 **161(1)** 1025-1029.
[19] Peyghan AA, Omidvar A, Hadipour NL, Bagheri Z, Kamfiroozi M, *Can aluminum nitride nanotubes detect the toxic NH 3 molecules?* Physica E: Low-dimensional Systems and Nanostructures, 2012 **44(7)** 1357-1360.
[20] https://www.comsol.com/.
[21] Dewit R, "Elastic constants and thermal expansion averages of a nontextured polycrystal", Journal of mechanics of materials and structures, 2008 **3(2)** 195-211.
[22] Gao, Y. and Z.L. Wang, *Electrostatic potential in a bent piezoelectric nanowire. The fundamental theory of nanogenerator and nanopiezotronics.* Nano letters, 2007 **7(8)** 2499-2505.
[23] Moheimani SR. and Fleming AJ, *Piezoelectric transducers for vibration control and damping*. 2006: Springer Science & Business Media.